Research

Preparation, characterization and cooling performance of ZnO based Nanofluids

Muzaffar Hussain[1,2] · M. A. Ansari[2] · Feroz A. Mir[3]

Abstract

Nanoparticles (NPs) of Zinc Oxide (ZnO) were synthesized by the sol–gel method. These NPs were characterized for structural vibrational, morphological, optical, and electrical properties by X-ray diffraction (XRD), Fourier Transform infrared (FT-IR) spectroscopy, Scanning Electron Microscopy (SEM), UV–Visible optical absorption spectroscopy, and dielectric spectroscopy. Structural analysis confirms that all the NPs have a single-phase rutile tetragonal structure. Also from the Scherer formula, the average particle size for this compound was found to be around 10.25 nm. From SEM images, the observed NPs are spherical in shape, with an average size ranging from 10 to 100 nm. FT-IR data indicates a Zn–O vibrational bond and confirms the ZnO structure. Further, according to the optical data analysis, these NPs show an optical band gap of around 3.27 eV and follow an indirect transition. The dielectric constant (ε_r) and loss constant (ε) show good dispersion with the applied frequency. Also using these NPs, a nanofluid in transformer oil (mineral oil) was prepared. Further ε_r & ε_i shows good variation with the contents of NPs in the mineral oil. This nanofluid was tested for the cooling of transformers and shows some encouraging results. Based on these results, this material seems like a good candidate for transformer insulation and cooling applications.

Article Highlights

- The ZnO NPs were prepared by the sol-gel method.
- The prepared NPs showed a wurtize crystal structure with a particle size of around 10.25nm and an optical band gap of approximately 3.27 eV.
- The NPs were mixed with transformer oil to form nanofluid and were further used for cooling purposes in transformers, showing good performance. Therefore, it could be used in this promising field.

✉ Muzaffar Hussain, muzaffarh8@gmail.com; ✉ Feroz A. Mir, famirnit@gmail.com | [1]Department of EE, Baba Ghulam Shah Badshah University (BGSBU), Rajouri, Jammu and Kashmir 185234, India. [2]Department of EE, Gautam Buddha University (GBU), Greater Noida 201310, India. [3]Department of Physics, Baba Ghulam Shah Badshah University (BGSBU), Rajouri, Jammu and Kashmir 185234, India.

Discover

1 Introduction

Insulating liquids are extensively utilized to avert damage to high-voltage (HV) electrical components, including tap changers, transformers, cables, reactors, power capacitors, circuit breakers, and bushings [1]. These liquids must, among other things, enable insulation and heat transfer in HV power transformers, which are essential parts of the transmission and distribution of electrical energy networks. The expected life of transformers is halved in HV transformers due to insulation problems, which account for 75% of all transformer failures [2]. Considering that pressboard and paper are solid insulators, as well as the insulating fluid (transformer oil) in the insulation system [2].Transformer oils are primarily used for cooling, corrosion prevention, electrical insulation, and reliable insulation protection against air and moisture [2].

Mineral oils are the insulating liquids most frequently employed in transformers. Because of their affordability, dielectric and cooling qualities, compatibility with cellulose-based solid insulation materials, and availability, they have been marketed and used since the turn of the twentieth century [3]. Mineral oils have many common advantages; however, they also have a number of detrimental qualities, such as being flammable, having low biodegradability, having a low moisture tolerance, and having corrosive sulphur compounds [4]. Low flash and fire temperatures can lead to heat protection concerns, so it's important to use firewalls, deluge systems, and fire safety measures [5]. Mineral oils are a byproduct of the oil industry and are composed of several hydrocarbon molecules. Oil reserves will eventually run out; according to some predictions, there will be an oil scarcity in the middle of the twentieth century [3]. It will pose a serious threat to the industry that consumes billions of liters of insulating liquids [1].

Over the past 40 years, numerous studies of substitute insulating liquids have been conducted in an effort to minimize the issues associated with these drawbacks [6, 7]. These alternative liquids are anticipated to meet a number of specifications, including better fire safety, good sustainability, prolonged service life, high dielectric strength, and good heat transmission [8, 9].

In the middle of the 1990s, nanoparticles (NP) were added to insulating liquids to find a new nanofluid that enhanced their thermal and electrical properties compared to mineral oil [9]. Enhancing thermal qualities, including diffusivity, conductivity, convective coefficient, and heat transfer, was the primary goal of the first generation of nanofluids (NFs) or fluids containing nanoparticles [10]. Some nanoparticles allow for the improvement of fluid dielectric strength in addition to their enhancement of thermal properties. NFs are, therefore, a perfect substitute insulator for oil-filled high-voltage applications [11]. Transformer oils with NP added provide several advantages, including longer insulation and transformer life, enhanced partial discharge characteristics, enhanced AC, DC, and impulse breakdown performances, higher thermal conductivity, and better cooling of transformers [8]. The thermal performance analysis was conducted on different metal oxide water-based nanofluids, and it has been found that the nanofluid shows improvements in heat transfer capability and is a better solution for different cooling systems [12].

The future is the age of nanotechnology, and the novel properties of nanomaterials make them suitable candidates for developing nanomaterials effectively by synthesis process. Among the various featured materials, oxide-based nanomaterial's are at the center of the research community. For the last few decades, oxide-based semiconductors, specifically Tin dioxide (ZnO), have been in prime focus due to their specific properties (like optical, magnetic, and electrical) [13]. Due to their traditional qualities and anticipated future uses, zinc oxide (ZnO)-based nanostructures have taken center stage among metal oxide nanostructures over the past few decades [14, 15]. The crystal structure of bulk ZnO is typically tetragonal rutile, with a P42/mnm space group, two Sn, and four oxygen atoms in each unit cell. Bulk ZnO can be synthesized with lattice parameters of $a = b = 0.4737$ nm and $c = 0.3185$ nm. ZnO is a wide-energy-gap n-type semiconductor with a high carrier concentration (6×10^{20} cm^{-3}) and an optical band gap (Eg) of 3.27 eV at 300 K. It thus foresees the potential applications of its range, which include optoelectronic devices, Li batteries, transparent conducting electrodes, and gas sensors. The impact of several geometrical morphologies on ZnO's physical properties, including NPs, nanobelts, nanowires, nanorods, nanodiskettes, and nanoflowers, has been studied [7, 9–11, 13–15]. Notably, the number of defects, oxygen vacancies, and surface morphology all has a significant role in determining the electrical characteristics of ZnO [9–11]. ZnO can be utilized in transformer oil because of its electric and optical characteristics. The effect of doping, film formation, nanostructure, and production process on various physical properties is discussed in a sizable number of these ZnO studies [13–16].

Although ZnO NPs have been researched by a number of academics, there hasn't been a complete or in-depth investigation of using them as nanofluids for cooling purposes.TiO$_2$ and ZnO are used in over 30% of the studies on naturally occurring ester–based nanofluids in the literature [17]. However, these studies remain limited to dielectric constant and breakdown voltages. Therefore, the current investigation carried out on ZnO-based nanofluids is

induction heating-based. Further, the effect of magnetic fields on the nanofluid has not been reported in the literature. This is the first ever report regarding induction heating.

Based on these various studies carried out on ZnO NPs, here we prepared ZnO NPs by the sol–gel method. These particles were characterized by various standard techniques. Further, these NPs were used in transformers as nanofluids for cooling purposes. Hence, based on various steps, from preparation to characterization, the current paper is divided into various sections and sub-sections. Like the section I contain reports from the literature on nanofluids. Section II shows experimental materials and methods. In this section, steps involved in the preparation and characterization of NPs are given. Section III presents results and discussions. This section is divided into different subsections, like XRD, where crystallographic parameters related to materials are given and discussed. In another subsection, the manuscript discusses the SEM studies of the material; further sections discuss the FTIR optical absorption, dielectric, and breakdown study of NPs and nanofluid. Final Section IV gives the conclusion related to the current work.

2 Experimental (materials and methods)

Using analytical grade 2 Molar of zinc acetate ($ZnCHCOOH.2H_2O$), i.e., 6.57 g, and 0.5 Molar of sodium hydroxide (NaOH), i.e., 0.399 g, as starting materials, ZnO NPs are synthesized using the sol–gel method. The aforementioned material is dissolved in deionized water in stoichiometric proportions. After that, a certain amount of polyethylene glycol (PEG, Mw = 400) is added to the solution while it is continuously stirred for roughly 20 min. Following that, the solution is heated at 80 °C to get pH values as high as 8–10 and enable the gel to form. A milky-colored gel was formed, and any organic impurities were removed by repeatedly washing it in double-distilled water and ethanol. To eliminate any remaining organic material, this gel was heated for six hours at 300 °C after being dried for 12 h in an air oven at 90 °C. A portion of the powdered material was combined with polyvinyl alcohol (PVA) and allowed to dry overnight after being ground for 30 min. This PVA-containing mixture was then forced into disk-shaped pellets using a hydraulic press, which exerted a pressure of around four tons. The pressed samples were sintered in the air for six hours at 600 °C. The phase formation and crystal structure determination were carried out using a RIGAKU X-ray powder diffractometer with Cu K radiation (λ = 1.54056A°) at a scanning rate of 2°/min, ranging from 20° to 75°. The morphological study was done using scanning electron microscopy (SEM) (Hitachi, Model S-4300). The Fourier transform infrared (FTIR) spectroscopy of these samples was investigated by the Agilent Cary 630 spectrometer. These optical absorption studies of this sample were carried out using a dual-beam photo spectrometer (Shimadzu, UV-1601).

Two methods are used to synthesis nanofluids: the single-step approach and the two-step method. For large-scale production of nanofluids, the two-step technique is the most economical [18, 19]. In this work, a mineral oil-based nanofluid was prepared using the two-step method. Different concentrations of ZnO nanoparticles—0.1, 0.2, and 0.3 g/L—are taken and dispersed in the transformer oil. After 30 min of continuous stirring with a magnetic stirrer, the mixture was sonicated to ensure good dispersion. The sonication helps to reduce any bubble formation (and is a good source of moisture) in the sample [9, 20, 21].

The dielectric response of nanofluid was checked using a high- precision LCR meter (Scientific Model SM 6023) in cylinder capacitor geometry with a frequency range of 20 Hz to 5 kHz at room temperature. The dielectric breakdown of all nanofluid samples was conducted in a breakdown tester and per IEC 60156 [10]. The two electrodes (copper) fitted in the cup oil tester were spherical in shape with 2.5 mm of space between them, and the capacity of the cup was 300 ml. During the test, the electrodes were wholly immersed in the oil. The voltage applied across the electrodes is raised at a rate of 2 kV/sec. The test was repeated five times for each sample. The gap between each test was 5 min (in order to stabiles the system), and the average value of the breakdown was taken.

For induction heating measurements, a certain concentration of nanofluid was taken in a test tube and kept in a custom-designed solenoid. This coil was connected to the Hysteresis Loop Tracer (Scientech India, Model Nvis6108). This setup is a variable AC power supply (with a fixed frequency of 50 Hz) producing different currents and hence an AC magnetic field. The exposure was done for different time intervals at different AC magnetic fields, and corresponding change in temperature in the nanofluid was noticed by using a digital thermometer.

Fig. 1 **a** XRD of ZnO Nanoparticles and **b** Structure of ZnO
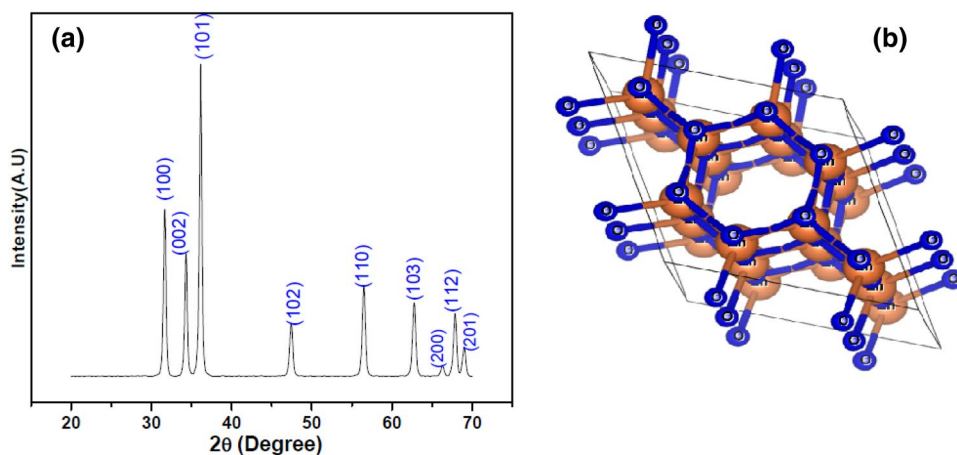
3 Results and discussion

3.1 Structural analysis

Figure 1a depicts the ZnO NPs' XRD patterns. These samples' XRD patterns reveal a series of prominent peaks with hkl (Miller indices) *(110), (101), (200),* and *(211)* that, respectively, correlate to 2θ at 26°, 34°, 38° and 52°. In each case, the rutile phase of ZnO with a tetragonal crystal structure was visible. These samples' observed peaks are in good agreement with JCPDS file no. 88–0287, which depicts the rutile structure of ZnO NPs [2–4, 8]. However, it has been noticed that the peaks are slightly stretching, lowering intensity, and shifting toward their higher diffracting angles. The observed peak broadening is consistent with decreased particle size. Since ZnO has a tetragonal crystal structure, the lattice parameters a and c of ZnO NPs have been computed using the following relation:

$$1/d = \left(h^2 + k^2\right)/a + l^2/c \qquad (1)$$

where *d* is lattice spacing in Å. The *d* values have been calculated using the (110) peak for different ZnO matrix values. Also in nanostructures, particularly in the case of NPs, changes may be caused by lattice compression brought on by microstrains [22–27]. The possible reason could also be the large aspect ratio of the NPs (surface-to-volume ratio) and the existing micro-strains that the surface-solid solution of ZnO can create.

The Scherer formula [28] can be used to determine the crystallite size from the diffraction lines of the (1 1 0) planes.

$$D = K\lambda/\beta_{hkl}\cos\theta \qquad (2)$$

where K is a shape factor (0.89), λ is the X-ray wavelength (1.543 Å for Cu K_α), β_{hkl} (full width at half maximum) $= (\beta^2_M - \beta^2_i)^{1/2}$. β_M and β_i are the measured and instrumental broadening in radians, respectively, and θ is Bragg's angle in degrees. The current ZnO NP has an estimated crystallite or grain size of 10.25 nm. The fundamental rutile phase, as previously mentioned, basically stays the same. Additionally, this in the ZnO matrix will disrupt the system's numerous physical properties and cause the disorder.

Broadening peaks typically indicate an increase in the concentration of lattice imperfections because the internal micro-strain within the crystal matrix has decrease other researchers endorse the same conduct [29]. Smaller strain and dislocation densities are further correlated with smaller grain sizes, which further increase the matrix's imperfect regions.
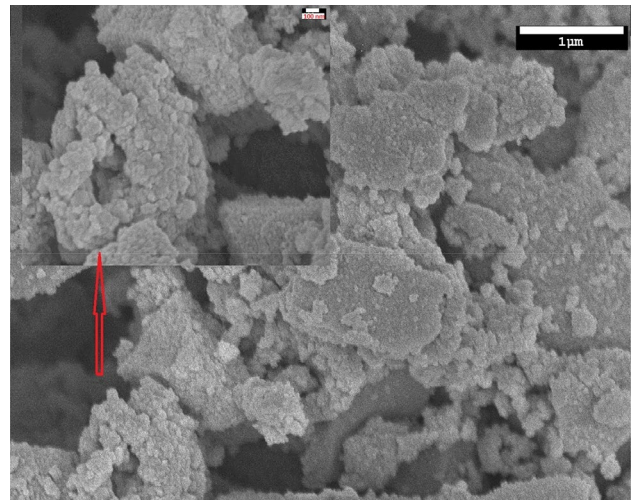
The strain (ε) induced in samples due to crystal imperfections and distortion was computed using the following formula [30]:
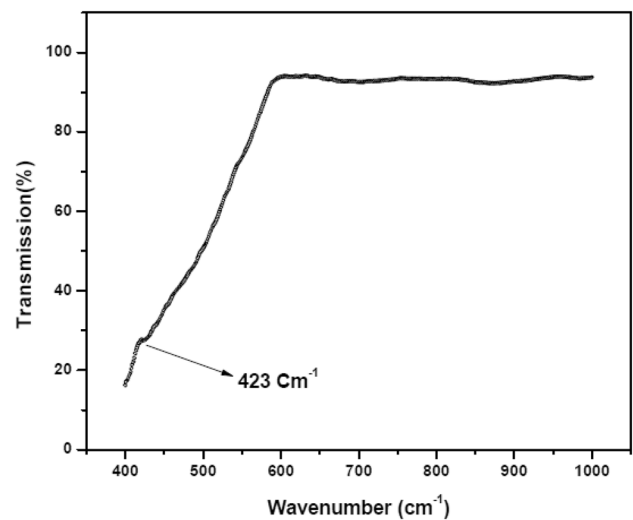
$$\varepsilon = \beta_{hlk}/4\tan\theta \qquad (3)$$

The dislocation density (δ), defined as the length of dislocation lines per unit volume of the nanocrystal, was estimated using the following formula [30]:

$$\delta = 1/D^2 \qquad (4)$$

Fig. 2 SEM Images of ZnO NPs. Inset show a zoomed area with a 100 nm scale

Fig. 3 FTIR of ZnO Nanoparticles

It should be mentioned that strain and dislocation density are indicators of a matrix dislocation network; an increase in dislocation density denotes the creation of a high-quality compound. However, the strain that resulted from nanoformation means that the present system has less crystallinity and more disorder. For the current sample, the observed rising value of β_{hkl} points to a decline in crystalline quality. Additionally, the observed non-homogeneous strain component may appear at the sub-grain, crystallite, or subdomain level close to the grain.

3.2 Morphological study

SEM was used to examine the surface morphology of the prepared sample. Figure 2 shows the SEM images for ZnO NPs. Every particle has a smooth, fully spherical surface within the studied/focusing area/range (more accurately, these photos demonstrate that the pure ZnO NPs material was uniform and spherical). Also, these particles seem to be aggregated with smaller nanoparticles ranging from 10 to 100 nm. The surface seems compact.

3.3 FTIR study

The FTIR spectra of the ZnO NPs are displayed in Fig. 3. The spectra exhibit the clearly defined characteristic peaks of the ZnO-related stretching vibration bands at 618 cm^{-1} and 421 cm^{-1} [30, 31]. Additionally, the Zn–O stretching mode is shown by the absorption band at 423 cm^{-1} [31]. Strong chemical bonding in ZnO NPs is indicated by a shift in the bands that have been seen. This also suggests that the ZnO structure is formed.

Discover

Fig. 4 Right shows Uv–visible spectra of ZnO Nanoparticles and left shows its Tauc plot
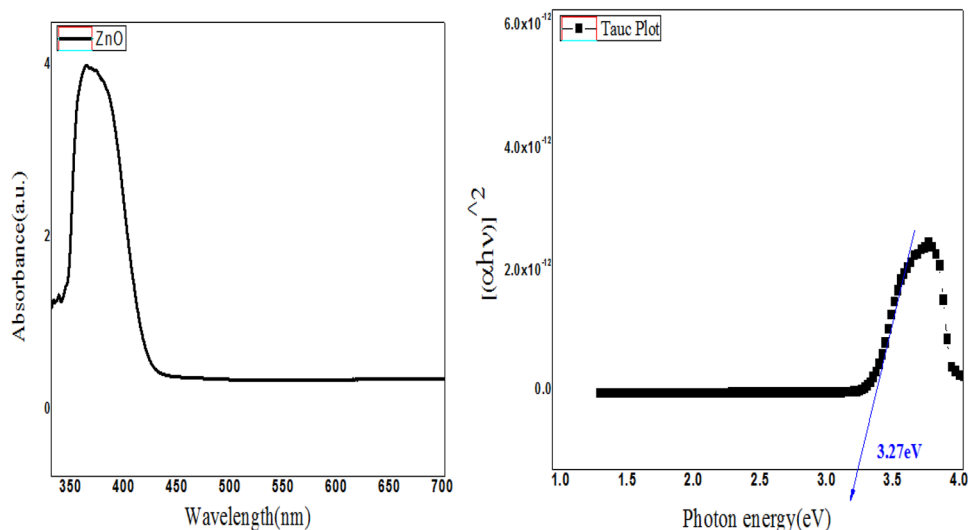
3.4 Optical study

A broad absorption peak with a maximum at 300–550 nm regions can be observed in the UV–visible spectra. Compared to the bulk ZnO NPs, the absorption peak at 350 nm is blue-shifted. Due to the system's exactions' quantum confinement, the absorption edge has been blue-shifted. The quantum confinement of the ZnO NPs in the present scenario may be the primary cause of the broadening of the absorption spectra. The size of the crystallites also affects the quantum confinement's outcome. The order of confinement and its effect improve as the size of the particles decreases. Energy can transfer to the atom effectively due to its confinement in a nanocrystalline structure. This works in tandem with that system to create a new energy level within ZnO's band structure.

The Tauc equation was used to determine the optical energy gap of irradiated samples [32].

$$(\alpha h\upsilon)^{1/n} = B(h\upsilon - E_g) \tag{5}$$

where "n" is the exponent indicating the type of electron transition in the system,"α" is the absorption coefficient, "$h\upsilon$" is the energy (h is a Planks constant with a value of 6.625×10^{-34} J/s and υ is the frequency of the photon in Hz) of the incident photon, and E_g is the value of the optical band gap. For direct and indirect permissible transitions, n typically takes values of 1/2 and 2, respectively. Furthermore, factor B is a constant that relies on the transition probability. Extrapolating the experimental curve's $(\alpha h\upsilon)^n$ to the x-axis linear range yields the energy magnitude. Plotting $(\alpha h\upsilon)^n$ against $h\upsilon$ is typically used to calculate the value of Eg (Tauc plot). In this work, the band gap energy was computed using the value of n = 2.Band gaps for ZnO NPs have been calculated by extrapolating the straight part of this relation to the $h\upsilon$ axis (Tauc plot, depicted in the inset of Fig. 4). Due to its nanosize, the system exhibits a small reduction in the optical band gap. Due to the quantum size effect, the obtained value, in this case, is lower than that of bulk ZnO (3.27 eV). The results from the UV–vis spectra align with those from the XRD [33–37].

These nanocomposites' Urbach band tail (also called defect tail) was also evaluated. Sub-gap absorptions (sub-band states) are thoroughly studied using this Urbach energy. The Urbach rule was used to calculate the Urbach energy (Eu) [32].

$$\alpha = \alpha_0 \exp(h\upsilon)/E_u \tag{6}$$

where α_0 represents the pre-exponential absorption coefficient factor. It should be emphasized that there are numerous causes for the Urbach band tail in semiconductors, including the carrier phonon interaction, carrier-impurity interaction, and structural disorder [31]. The values of Eu are obtained from the inverse slope of the straight line, which represents $ln(\alpha)$ vs photon energy ($h\upsilon$), by fitting Eq. (6). (Figure not shown here). Therefore, the defect energy's magnitude increases

Fig. 5 Dielectric of the Nano-fluid with different concentration ZnO Nanoparticles
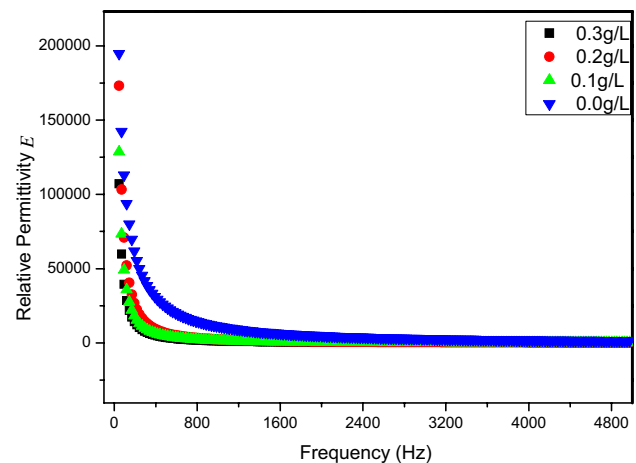
as Eg decreases. The narrowing of Eg, however, may result from sub-band states that occur between the valence and conduction bands in nanostructure formation. Additionally, the quantity of defect states/levels below the conduction band rises to the point where the band edge is deeply displaced into the forbidden gap, lowering the effective Eg of the current system. Thus, it was abundantly evident that the primary cause of this observed behavior may be the increase of pre-existing defects or disorders after particle size reduction.

The Effective Mass Approximation (EMA) model (Brus equation) approach can also be used to calculate the size of nanoparticles using optical absorption data [33].

$$E = E_{Bulk} + h^2\pi^2/2\,e\,r^2\left(1/m_e + 1/m_h\right) \tag{7}$$

where r is the particle radius, m_e and m_h are the effective masses of the electrons and holes, m_0 is the free electron mass, E is the band gap of the NPs, and E_{bulk} is the band gap of the bulk material, $m_e = 0.34\,m_0$, $m_h = 0.23m_0$, and $\varepsilon_r = 8.76$ are the sample's permittivity values in this case. Equation (7) was additionally applied to determine the size from the UV–Vis absorption data of ZnO NPs, and in current case, it was found to be around 8.2 nm. Since the positions of the peaks may be connected to the average particle diameter, a smaller diameter indicates a shorter wavelength (blue shift).The Quantum Size Effect (QSE) produced by these NPs is confirmed. According to QSE in direct-gap semiconductor nanocrystals, the optical absorption edge shifts to higher energies with decreasing size, which can account for the UV–Vis red-shift effect [33]. The average nanoparticle size measured using XRD data and that inferred from the optical data analysis are in good agreement. The sensitivity of the procedure may be the cause of a little difference in size calculation between the two techniques.

3.5 Dielectric study

By using dielectric spectroscopy, several research on the polarization and relaxation processes in nanofluids were confirmed [38]. In polar liquids or solid polar liquid mixtures, polarization due to molecular rotation; polarization due to charge accumulation at the interfaces of different media in colloidal suspension; polarization due to ion atmosphere displacement; and polarization due to diffusion coupling between ion flows are the potential causes of the frequency-dependent change in relative permittivity and dissipation factor [39–41]. The real permittivity of a pure transformer decreases exponentially with the increase in frequency from 20 Hz and becomes constant at a higher frequency, as shown in Fig. 5. The addition of different concentrations (0.1, 0.2, & 0.3 g/L) of ZnO nanoparticles causes a decrease in the real permittivity. The permittivity of all concentrations is less as compared with pure transformer oil. However, the nanofluid with a concentration of 0.2 g/L shows more permittivity than 0.1 g/L and 0.3 g/L nanofluid concentrations. This decrease is due to the interaction zones between transformer oil and nanoparticles. It has been reported that in response to variations in the base fluid, nanoparticle size, shape, concentration, pH, change in temperature, the nanofluid exhibits significant changes in its thermophysical as well as rheological features [42, 43].

Fig. 6 AC breakdown voltage of transformer oil, Transformer oil with 0.1 g/L, 0.2 g/L, and 0.3 g/L of ZnO
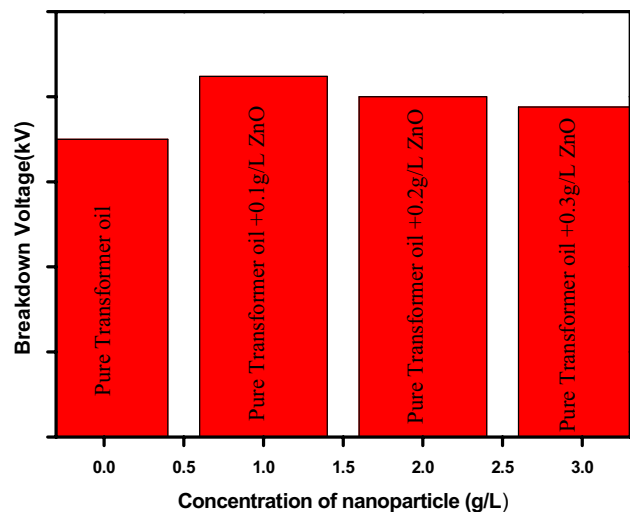
Table 1 Percentage increase in breakdown voltage upon adding different concentration of ZnO

S.No.	Dielectric liquid	Breakdown voltage (BDV)	% increase in BDV
1	Transformer oil	35	–
2	Transformer oil + 0.1 g/L ZnO	42.4	21.1
3	Transformer oil + 0.2 g/L ZnO	40	14.2
4	Transformer oil + 0.3 g/L ZnO	38.8	10.85

3.6 Breakdown of nanofluid

The dielectric strength of the transformer oil is one of the essential features of the transformer. Thus, the breakdown voltage performance of transformer oil with and without nanoparticles is experimentally assessed. Typically, an average value is calculated to determine the quality of transformer oil. However, transformers are designed to withstand the minimum voltage level of insulation instead of the mean withstand voltage. Figure 6 shows the breakdown voltage with different concentrations of nanofluid. The 0.1 g/L nanofluid concentration shows improved breakdown voltage compared with pure transformer oil, and as well as that of 0.2 g/L and 0.3 g/L nanofluid concentrations. Improvements in breakdown voltage are also shown in Table 1. Further, other researchers have used different types of nanoparticles in different base fluids and have taken different concentrations of nanoparticles in their respective base fluids. Hence, makes it difficult to compare it with the current results. However, majority of studies show improvements in breakdown voltages with the addition of nanoparticles [11].

3.7 Induction heating study

Figure 7a–e demonstrates the heating capacity of various concentrations of nanofluid and pure transformer oil measured at a fixed frequency of 50 Hz for 1 h for different samples under various magnetic field strengths ranging from 55 to 121 Oe. At a low magnetic field, the temperature of all samples increases as compared with pure transformer oil. The reason is that ZnO shows weak paramagnetic behavior; the unsaturated spins got oriented by the magnetic field and dissipated energy, causing an increase in fluid temperature. With the increase in a magnetic field, the temperature rise in nanofluid is less than that in pure transformer oil because the spins get permanently orientated at the higher magnetic field [44]. Also, the melting point and band gap of ZnO are quite high and hence absorb more heat energy [45]. One of the possible reasons could be the aspect ratio of the nanoparticles, which can help absorb more heat. The temperature rise with the change in the magnetic field is less for 0.1 g/L concentration as compared

Fig. 7 a–e shows the induction heating of a pure transformer oil and nanofluid of different concentrations and under different magnetic fields
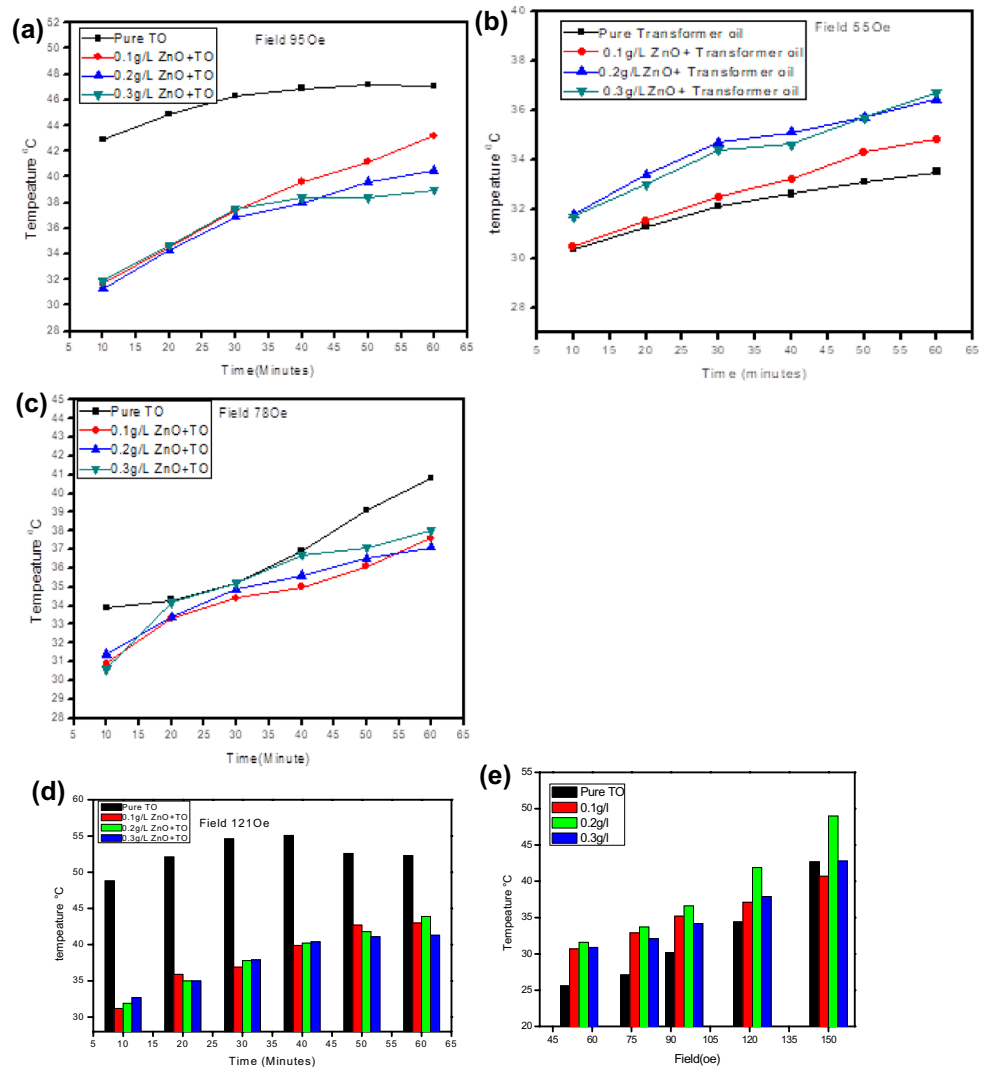
with 0.2 g/L and 0.3 g/L. This measurement here projects that the 0.1 g/L concentration is the optimal concentration for transformer cooling purposes.

4 Conclusion

The sol–gel method was used to synthesize the tetragonal phase of ZnO NPs. The NPs' typical crystallite sizes were discovered to be in the range of 10.25 nm. At room temperature, the dielectric characteristics behave normally with frequency. The hopping of charges and polarization of the interfacial space charges have been used to explain the conductivity and dielectric behavior. These NPs show consistent dielectric loss behavior at higher frequencies, which suggests that they are lossless materials. To examine the impact of ZnO on the breakdown voltage of transformer oil, three quantities of ZnO nanoparticles (0.1 g/L, 0.2 g/L, and 0.3 g/L) are introduced to transformer oil. According to research, when compared to other nanofluid concentrations, 0.1 g/L concentration has a higher breakdown voltage. Additionally, 0.1 g/L yields the greatest results in a study on induction heating of the material. In light of the aforementioned findings, it is additionally recommended that these NPs might be utilized in high-frequency electrical device applications.

Declarations

Competing interests We don't have any competing interests related with this paper.

References

1. Rafiq MI, et al. Use of vegetable oils as transformer oils—a review. Renew Sustain Energy. 2015;52:308–24. https://doi.org/10.1016/j.rser.2015.07.032.
2. Rafiq M, Chengrong L, Lv Y. Effect of Al2O3 nanorods on dielectric strength of aged transformer oil/paper insulation system. J Mol Liq. 2019;284:700–8. https://doi.org/10.1016/j.molliq.2019.04.041.
3. Lv Y, et al. Fabrication, characterization, and insulating property of Fe3O4 nanofluids. Integr Ferroelectr. 2017;180(1):37–43. https://doi.org/10.1080/10584587.2017.1336790.
4. Wang Q, et al. Preparation of three types of transformer oil-based nanofluids and comparative study on the effect of nanoparticle concentrations on insulating property of transformer oil. J Nanotechnol. 2016. https://doi.org/10.1155/2016/5802753.
5. Mergos JA, et al. Dielectric properties of nanopowder dispersions in paraffin oil. IEEE Trans Dielectr Electr Insul. 2012;19(5):1502–7. https://doi.org/10.1109/TDEI.2012.6311493.
6. Negri F. Fundamental study and modeling of nanofluids, Ph.D. Thesis, University of Bologna, School of Electrical Engineering, 2017 Modern Physics Letters B. 2011; 25(25): 2012–2031.
7. Zhong Y, et al. Insulating properties and charge characteristics of natural ester fluid modified by TiO2 semiconductive nanoparticles. IEEE Trans Dielectr Electr Insul. 2013;20(1):135–40. https://doi.org/10.1109/TDEI.2013.6451351.
8. Herchl F, et al. Breakdown and partial discharges in magnetic liquids. J Phys Condens Matter. 2008;20(20):204110. https://doi.org/10.1088/0953-8984/20/20/204110.
9. D1533 AS. Standard test method for water in insulating liquids by Coulometric Karl fischer titration. ASTM International. 2012. https://doi.org/10.1520/D1533-00R05
10. Baur M et al. Insulating liquids breakdown voltage determination: test method efficiency. In 2017 IEEE 19th International Conference on Dielectric Liquids (ICDL). 2017. https://doi.org/10.1109/ICDL.2017.8124657
11. Hussain M, Mir FA, Ansari MA. Nanofluid transformer oil for cooling and insulating applications: a brief review. Appl Surface Sci Adv. 2022;8:100223. https://doi.org/10.1016/j.apsadv.2022.100223.
12. Loong TT, et al. Thermal performance evaluation for different type of metal oxide water based nanofluids. Case Stud Therm Eng. 2021;27:101288. https://doi.org/10.1016/j.csite.2021.101288.
13. Hartnagel, H.L., Semiconducting transparent thin films. 1995, Institute of Physics Publishing, Bristol and Philadelphia.Corpus ID: 265860822
14. Anderson JWJE, Handbook of Chemistry and Physics (Forty-Fourth edition), edited by C. D. Hodgman, R. C. Weast, and S. M. Selby. Pp. xxv + 3481.The Chemical Rubber Publishing Co., Cleveland, Ohio.1961. $12; $12.50 outside U.S.A. 1962.**21**: p. 59.ASIN : B000WQJ5D0
15. Bârsan N, Weimar U. Understanding the fundamental principles of metal oxide based gas sensors; the example of CO sensing with SnO2 sensors in the presence of humidity. J Phys Condens Matter. 2003;15(20):R813. https://doi.org/10.1088/0953-8984/15/20/201.
16. Hanai M et al. Dependence of TiO2 and ZnO nanoparticle concentration on electrical insulation characteristics of insulating oil. In 2013 Annual Report Conference on Electrical Insulation and Dielectric Phenomena. 2013. https://doi.org/10.1109/CEIDP.2013.6748164
17. Duzkaya H, Beroual A. Statistical analysis of AC dielectric strength of natural ester-based ZnO nanofluids. Energies. 2020;14(1):99. https://doi.org/10.3390/en14010099.
18. Zakaria IH, et al. Characteristics of mineral oil-based nanofluids for power transformer application. Int J Electr Comput Eng. 2017;7:1530–7. https://doi.org/10.11591/ijece.v7i3.pp1530-1537.
19. Jin H. Dielectric strength and thermal conductivity of mineral oil based nanofluids, in electrical engineering, mathematics and computer science. Delft University of Technology, Netherlands. 2015. https://doi.org/10.4233/uuid:10d18961-a23f-478e-b6e2-181d897d8541
20. Muangpratoom P et al. Dielectric properties of mineral oil-based nanofluids using zinc oxide nano-composites for power transformer application. In 2018 Condition Monitoring and Diagnosis (CMD). 2018. https://doi.org/10.1109/CMD.2018.8535968

21. Han Z. Nanofluids with enhanced thermal transport properties, in department of mechanical engineering. 2008, University of Maryland at College Park: College Park, Maryland.Corpus ID: 135019899

22. Ristić M, et al. Sol–gel synthesis and characterization of nanocrystalline ZnO powders. J Alloy Compd. 2005;397(1):L1–4. https://doi.org/10.1016/j.jallcom.2005.01.045.

23. Borysiewicz M. ZnO as a functional material, a review. Crystals. 2019;9:505. https://doi.org/10.3390/cryst9100505.

24. Liu C, Yun F, Morkoç H. Ferromagnetism of ZnO and GaN: a review. J Mater Sci Mater Electron. 2005;16(9):555–97. https://doi.org/10.1007/s10854-005-3232-1.

25. Levinson L, Philipp H. Zinc oxide varistors—a review. Am Ceram Soc Bull. 1986;65:639–46.

26. Kumar R, et al. Zinc oxide nanostructures for NO2 gas–sensor applications: a review. Nano-Micro Lett. 2015;7(2):97–120. https://doi.org/10.1007/s40820-014-0023-3.

27. Moezzi A, McDonagh AM, Cortie MB. Zinc oxide particles: synthesis, properties and applications. Chem Eng J. 2012;185–186:1–22. https://doi.org/10.1016/j.cej.2012.01.076.

28. Bhardwaj R, et al. Structural and electronic investigation of ZnO nanostructures synthesized under different environments. Heliyon. 2018;4(4):e00594. https://doi.org/10.1016/j.heliyon.2018.e00594.

29. Kumar S, Singh V, Tanwar A. Structural, morphological, optical and photocatalytic properties of Ag-doped ZnO nanoparticles. J Mater Sci Mater Electron. 2016;27(2):2166–73. https://doi.org/10.1007/s10854-015-4227-1.

30. Jagodzinski H, Klug HP, Alexander LE. X-ray diffraction procedures for polycrystalline and amorphous materials, 2. Auflage. John Wiley & Sons, New York-Sydney-Toronto 1974, 966 Seiten, Preis: £ 18.55. Berichte der Bunsengesellschaft für physikalische Chemie. 1975;79(6):553–553.

31. Al Abdullah K, et al. Synthesis of ZnO nanopowders by using sol-gel and studying their structural and electrical properties at different temperature. Energy Procedia. 2017;119:565–70. https://doi.org/10.1016/j.egypro.2017.07.080.

32. Muthukumaran S, Gopalakrishnan R. Structural, FTIR and photoluminescence studies of Cu doped ZnO nanopowders by co-precipitation method. Opt Mater. 2012;34(11):1946–53. https://doi.org/10.1016/j.optmat.2012.06.004.

33. Viezbicke BD, et al. Evaluation of the Tauc method for optical absorption edge determination: ZnO thin films as a model system. Phys Status Solidi B. 2015;252(8):1700–10. https://doi.org/10.1002/pssb.201552007.

34. Macdonald JR, et al. Impedance spectroscopy: theory, experiment, and applications. 3rd ed. Hoboken: Wiley; 2018.

35. Shaba EY, et al. A critical review of synthesis parameters affecting the properties of zinc oxide nanoparticle and its application in wastewater treatment. Appl Water Sci. 2021;11(2):48. https://doi.org/10.1007/s13201-021-01370-z.

36. Hatamie A, et al. Zinc oxide nanostructure-modified textile and its application to biosensing, photocatalysis, and as antibacterial material. Langmuir. 2015;31(39):10913–21. https://doi.org/10.1021/acs.langmuir.5b02341.

37. Sun X, et al. Application of nanoparticles in enhanced oil recovery: a critical review of recent progress. Energies. 2017;10(3):345. https://doi.org/10.3390/en10030345.

38. Rajňák M, et al. Dielectric response of transformer oil based ferrofluid in low frequency range. J Appl Phys. 2013. https://doi.org/10.1063/1.4816012.

39. Idogun AK et al. A review study of oil displacement mechanisms and challenges of nanoparticle enhanced oil recovery. In SPE Nigeria Annual International Conference and Exhibition. 2016. DOI: https://doi.org/10.2118/184352-MS

40. Negin C, Ali S, Xie Q. Application of nanotechnology for enhancing oil recovery—a review. Petroleum. 2016;2(4):324–33. https://doi.org/10.1016/j.petlm.2016.10.002.

41. Cotae C. Dielectric anisotropy in ferrofluids. J Magn Magn Mater. 1983;39(1):85–7. https://doi.org/10.1016/0304-8853(83)90405-5.

42. Shah TR, Koten H, Ali HM. Performance effecting parameters of hybrid nanofluids. Hybrid nanofluids for convection heat transfer. Hoboken: Academic Press; 2020. p. 179–213. https://doi.org/10.1016/B978-0-12-819280-1.00005-7.

43. Karagoz Y et al. The effect of using metallic nanoparticles as coolant. In tractor and construction machinery engines on performance and emissions. Recent Researches in Engineering Sciences. 2021; 158.

44. Espurz A, Alameda JM, Espurz-Nieto A. Magnetically induced dielectric anisotropy in concentrated ferrofluids. J Phys D Appl Phys. 1989;22(8):1174. https://doi.org/10.1088/0022-3727/22/8/024.

45. Yusuf NA, et al. Magneto-dielectric anisotropy in magnetic fluids determined from magneto-optical measurements. J Magn Magn Mater. 1995;149(3):373–9. https://doi.org/10.1016/0304-8853(95)00059-3.